Supplemental Information

Extended Experimental Procedures

Antibodies for confocal and conventional fluorescence microscopy and for Western blotting. Antibodies were purchased from Abcam: biotinylated anti-Ad-Hexon (#ab34374, final dilution 1/100), anti-Ad5 (#ab6982, final dilution 1/50). Anti-mouse CD68 and CD11b-specific antibodies were also from Abcam, UK. Secondary antibodies and reagents were from Jackson Immunoresearch: Cy2 or Cy3-labeled streptavidin, or donkey anti-rat or rabbit antibodies, Cy2-, Cy3- or HRP-labeled. For Western blot analyses, rabbit monoclonal antibody 4D4G (from Cell Signaling Technology, USA) was used to detect Ser396 phosphorylated mouse IRF3. Goat polyclonal antibody Cat#AF4454 from R&D Systems, USA, was used to detect total IRF3 in mouse samples.

Immunofluorescence analyses of tissues. Mice were euthanized and livers were collected, frozen in O.C.T. compound and stored at -80°C until processed. Five consecutive 6-8 μm sections at 4 depth levels in the liver were cut, air dried, fixed for 10 minutes in acetone at -20°C, air dried for at least 4 hours, re-hydrated in TBS for one hour, blocked in 2% N.S. for 1 hour and incubated with primary antibodies overnight at 4°C with or without 0.1% saponin depending on the antigen. Then, sections were incubated with HRP-labeled secondary antibodies for 1 hour. Slides were developed with ImmPact DAB or NovaRed substrates (Vector Laboratories), air dried, mounted, and analyzed on a Leica microscope. For immunofluorescence stainings, slides were immediately mounted after washing off the secondary antibodies. Images were taken using CCD camera-equipped Leica dual light fluorescent microscope. Four representative images were taken for each section cut from tissues at least 3 depth levels.

For the analysis of macrophage cell death *in vivo*, mice were injected with the indicated pathogen and then with 50 μg of propidium iodide (Sigma, Cat #81845) 5 to 15 minutes prior to tissue harvesting. Livers were collected, frozen in OCT and sectioned. Distribution and quantity of

PI-permeable cells were analyzed using fluorescence microscopy without any further section processing. Images of representative and defined fields were collected using the red-channel and slides were fixed in acetone and stained with CD68-specific antibodies to visualize macrophage distribution. Images of the same fields of liver sections that were previously collected in the red channel were re-taken using the green ($CD68^+$) channel and both images were super-imposed using Adobe Photoshop program to define the number of $CD68^+$ cells with PI-positive nuclei as described above. For each experimental setting, at least 500 $CD68^+$ cells were analyzed for PI-permeability for each strain.

Assessment of virus replication *in vivo* and histopathology and function of the liver. The amounts of alanine aminotransferase (ALT) and asparagine aminotransferase (AST) in the serum were determined 48 hours after virus infection at the Clinical Pathology Core laboratory of the University of Washington Medical Center using established protocols. To define gross anatomical changes in the liver, livers were harvested from mice 48 hours after the wild type HAdv5 virus infection, frozen in OCT, sectioned, and stained with hematoxyllin and eosin. Virus DNA concentrations in the liver after the virus infection were determined by quantitative real-time PCR. Primers specific to HAdv5 hexon gene (5'-GACTCCTAAAGTGGTATTGT-3' and 5'-ACACCTCCCAGTGGAAAGCA-3') were added to the power SYBR Green reaction mixtures (Applied Biosystems) and run on 7500 real-time PCR machine (Applied Biosystems) in absolute quantification mode with standards prepared from HAdv5 DNA that was spiked with mouse genomic DNA. Cycling conditions were 95^0C-1min, 60^0C-1.5min for 40 cycles. Results are shown as HAdv5 genome copies per 10 ng of total mouse liver genomic DNA.

Generation of mice deficient with Bax and Bak. To generate mice deficient in both BAK and BAX, $Bak^{-/-}Bax^{fl/fl}$ mouse strain #6329 was purchased from Jackson Laboratories and bred to *Tie2*-CRE transgenic mice (Schlaeger et al., 2005). In *Tie2*-CRE mice, the CRE recombinase is expressed

under the control of *Tie2* promoter and expressed only in hematopoietic and endothelial cells. The ablation of *Bax* alleles in hematopoietic compartment was verified by differential PCR analysis using DNA purified from peripheral blood or bone-marrow cells from progeny mice with genotypes $Bak^{-/-}$ $Bax^{\Delta/\Delta}Cre^{+}$. Mice, deficient in both Bak and Bax also exhibit spleenomegaly. Upon tissue harvesting for analyses, the spleen sizes were evaluated and recorded as an additional phenotypic marker of efficient ablation of Bak and Bax in hematopoietic compartment.

Analysis of plasma LDH. Mice were injected with HAdv or *L.monocytogenes* and at 30 min (for HAdv), and at 60 min (for *L.monocytogenes*) post infection, the blood was collected from *vena cava* upon tissue harvesting. Plasma samples where prepared from the whole blood and 10 μl aliquotes were immediately used in triplicate analyses for LDH activity using TOX7 "In vitro Toxicology Lactic Dehydrogenase Assay kit" from Sigma-Aldrich (St. Louis, MO) as described by the manufacturer without any modifications.

Legends to Supplemental Figures

Figure S1. Liver resident macrophages lose plasma membrane integrity after interaction with HAdv at various doses; relates to Figure 1. (A) Mice were infected with indicated doses of wild type HAdv (virus particles per mouse) and 45 minutes later PI was injected intravenously. Mice were sacrificed 15 minutes later, and livers were harvested, frozen in OCT and sectioned. The images of PI^{+} cells (red) were taken using conventional fluorescent microscopy on dry liver sections without any processing to avoid PI diffusion. Then, sections were fixed and stained with anti-CD68 antibody (green) and images of the same fields as for red channels were taken for green channels to visualize the distribution of $CD68^{+}$ liver macrophages. Note that numerous macrophages in the liver parenchyma became PI-permeable even at the lowest virus dose applied. $N = 4$. Representative fields are shown. Scale bar is 50 μm. **(B)** Infection of hepatocytes mouse *in vitro* and *in vivo* or mouse bone

marrow-derived macrophages *in vitro* with HAdv *per se* does not trigger necrotic cell death and instead results in efficient expression of a virus-encoded transgene. For the analyses shown, indicated doses of HAdv5-based vector, expressing GFP were used for cell infection. GFP expression was analyzed 24 to 48 h later. Representative fields are shown. N = 5. **(C-F)** The percentage of PI-permeable $CD68^+$ cells in the liver parenchyma of indicated gene-deficient mice 60 minutes after challenge with HAdv. N = 5. Error bars represent standard deviation of the mean.

Figure S2. Confocal and electron microscopy analyses of HAdv interaction with $CD68^+$ liver macrophages after intravenous virus injection into *WT* and IRF3-deficient mice; relates to Figure 2. (A) Confocal microscopy analysis of liver sections of WT and IRF3-deficient mice after staining of the sections with anti-CD68-Mab (green), anti-HAdv Ab (red) and DAPI (blue). Note that $CD68^+$ cells in the livers of both *WT* and $Irf3^{-/-}$ mice efficiently accumulate HAdv particles (indicated by arrows). **(B, C)** Ultrastructural changes observed in macrophages of the $Irf3^{-/-}$ mice after challenge with HAdv, analyzed by transmission electron microscopy. $Irf3^{-/-}$ mice were injected with $5x10^{11}$ vp kg^{-1} of HAdv and 15 minutes later, animals were sacrificed and livers were harvested and processed for transmission electron microscopy. In mock-infected groups of wild type mice (WT-Mock) **(B)**, mice were injected with saline. Note that macrophages in virus-injected $Irf3^{-/-}$ group **(C)** contain mitochondria with normal morphology (blue arrows). However, numerous double membrane-layered vacuoles are present in the cytosol of virus-containing cells. The HAdv particles are shown by red arrows. Double membrane leyer vesicles are shown by green arrows. Representative images are shown. N = 3.

Figure S3. Distribution of PI-permeable cells on sections of the livers of *WT* and IRF3-deficient mice after infection with indicated pathogens; relates to Figure 3. Wild type (*WT*) and $Irf3^{-/-}$ mice were infected with indicated pathogens. After 45 minutes for HAdv2 and *ts1* viruses, and after 60 minutes for *L.monocytogenes* and Δ*hly* infection, livers were harvested and frozen in OCT. Images of

representative fields were taken using fluorescence microscopy. *N* = 5. Mock – mice were injected with saline. Scale bar is 50 μm.

Table S1. Mouse strains used in the current study (relates to all experiments).

Supplemental References (Relate to Table S1)

Berube, C., Boucher, L. M., Ma, W., Wakeham, A., Salmena, L., Hakem, R., Yeh, W. C., Mak, T. W., and Benchimol, S. (2005). Apoptosis caused by p53-induced protein with death domain (PIDD) depends on the death adapter protein RAIDD. Proceedings of the National Academy of Sciences of the United States of America *102*, 14314-14319.

Ch'en, I. L., Beisner, D. R., Degterev, A., Lynch, C., Yuan, J., Hoffmann, A., and Hedrick, S. M. (2008). Antigen-mediated T cell expansion regulated by parallel pathways of death. Proceedings of the National Academy of Sciences of the United States of America *105*, 17463-17468.

Hemmi, H., Kaisho, T., Takeuchi, O., Sato, S., Sanjo, H., Hoshino, K., Horiuchi, T., Tomizawa, H., Takeda, K., and Akira, S. (2002). Small anti-viral compounds activate immune cells via the TLR7 MyD88-dependent signaling pathway. Nature Immunology *3*, 196-200.

Hemmi, H., Takeuchi, O., Kawai, T., Kaisho, T., Sato, S., Sanjo, H., Matsumoto, M., Hoshino, K., Wagner, H., Takeda, K., and Akira, S. (2000). A Toll-like receptor recognizes bacterial DNA. Nature *408*, 740-745.

Horai, R., Asano, M., Sudo, K., Kanuka, H., Suzuki, M., Nishihara, M., Takahashi, M., and Iwakura, Y. (1998). Production of mice deficient in genes for interleukin (IL)-1 alpha, IL-1 beta, IL-1 alpha/beta, and IL-1 receptor antagonist shows that IL-1 beta is crucial in turpentine-induced fever development and glucocorticoid secretion. Journal of Experimental Medicine *187*, 1463-1475.

Hoshino, K., Takeuchi, O., Kawai, T., Sanjo, H., Ogawa, T., Takeda, Y., Takeda, K., and Akira, S. (1999). Cutting edge: Toll-like receptor 4 (TLR4)-deficient mice are hyporesponsive to

lipopolysaccharide: Evidence for TLR4 as the Lps gene product. Journal of Immunology *162*, 3749-3752.

Ishii, K. J., Coban, C., Kato, H., Takahashi, K., Torii, Y., Takeshita, F., Ludwig, H., Sutter, G., Suzuki, K., Hemmi, H., *et al.* (2006). A Toll-like receptor-independent antiviral response induced by double-stranded B-form DNA. Nature Immunology *7*, 40-48.

Kawai, T., Adachi, O., Ogawa, T., Takeda, K., and Akira, S. (1999). Unresponsiveness of MyD88-deficient mice to endotoxin. Immunity *11*, 115-122.

Kobayashi, K., Inohara, N., Hernandez, L. D., Galan, J. E., Nunez, G., Janeway, C. A., Medzhitov, R., and Flavell, R. A. (2002). RICK/Rip2/CARDIAK mediates signalling for receptors of the innate and adaptive immune systems. Nature *416*, 194-199.

Kuida, K., Lippke, J. A., Ku, G., Harding, M. W., Livingston, D. J., Su, M. S. S., and Flavell, R. A. (1995). Altered Cytokine Export and Apoptosis in Mice Deficient in Interleukin-1-Beta Converting-Enzyme. Science *267*, 2000-2003.

Mariathasan, S., Newton, K., Monack, D. M., Vucic, D., French, D. M., Lee, W. P., Roose-Girma, M., Erickson, S., and Dixit, V. M. (2004). Differential activation of the inflammasome by caspase-1 adaptors ASC and Ipaf. Nature *430*, 213-218.

Newton, K., Sun, X. Q., and Dixit, V. M. (2004). Kinase RIP3 is dispensable for normal NF-KBs, signaling by the B-cell and T-cell receptors, tumor necrosis factor receptor 1, and toll-like receptors 2 and 4. Molecular and Cellular Biology *24*, 1464-1469.

Oberst, A., Dillon, C. P., Weinlich, R., McCormick, L. L., Fitzgerald, P., Pop, C., Hakem, R., Salvesen, G. S., and Green, D. R. (2011). Catalytic activity of the caspase-8-FLIPL complex inhibits RIPK3-dependent necrosis. Nature *471*, 363-+.

Roth, W., Deussing, J., Botchkarev, V. A., Pauly-Evers, M., Saftig, P., Hafner, A., Schmidt, P., Schmahl, W., Scherer, J., Anton-Lamprecht, I., *et al.* (2000). Cathepsin L deficiency as molecular defect of furless: hyperproliferation of keratinocytes and pertubation of hair follicle cycling. Faseb Journal *14*, 2075-2086.

Salmena, L., Lemmers, B., Hakem, A., Matysiak-Zablocki, E., Murakami, K., Au, P. Y. B., Berry, D. M., Tamblyn, L., Shehabeldin, A., Migon, E., *et al.* (2003). Essential role for caspase 8 in T-cell homeostasis and T-cell-mediated immunity. Genes & Development *17*, 883-895.

Sarkar, A., Hall, M. W., Exline, M., Hart, J., Knatz, N., Gatson, N. T., and Wewers, M. D. (2006). Caspase-1 regulates Escherichia coli sepsis and splenic B cell apoptosis independently of interleukin-1 beta and interleukin-18. American Journal of Respiratory and Critical Care Medicine *174*, 1003-1010.

Schlaeger, T. M., Mikkola, H. K., Gekas, C., Helgadottir, H. B., and Orkin, S. H. (2005). Tie2Cre-mediated gene ablation defines the stem-cell leukemia gene (SCL/tal1)-dependent window during hematopoietic stem-cell development. Blood *105*, 3871-3874.

Shi, G. P., Villadangos, J. A., Dranoff, G., Small, C., Gu, L. J., Haley, K. J., Riese, R., Ploegh, H. L., and Chapman, H. A. (1999). Cathepsin S required for normal MHC class II peptide loading and germinal center development. Immunity *10*, 197-206.

Shornick, L. P., DeTogni, P., Mariathasan, S., Goellner, J., StraussSchoenberger, J., Karr, R. W., Ferguson, T. A., and Chaplin, D. D. (1996). Mice deficient in IL-1 beta manifest impaired contact hypersensitivity to trinitrochlorobenzene. Journal of Experimental Medicine *183*, 1427-1436.

Vasiljeva, O., Korovin, M., Gajda, M., Brodoefel, H., Bojic, L., Kruger, A., Schurigt, U., Sevenich, L., Turk, B., Peters, C., and Reinheckel, T. (2008). Reduced tumour cell proliferation and delayed development of high-grade mammary carcinomas in cathepsin B-deficient mice. Oncogene *27*, 4191-4199.

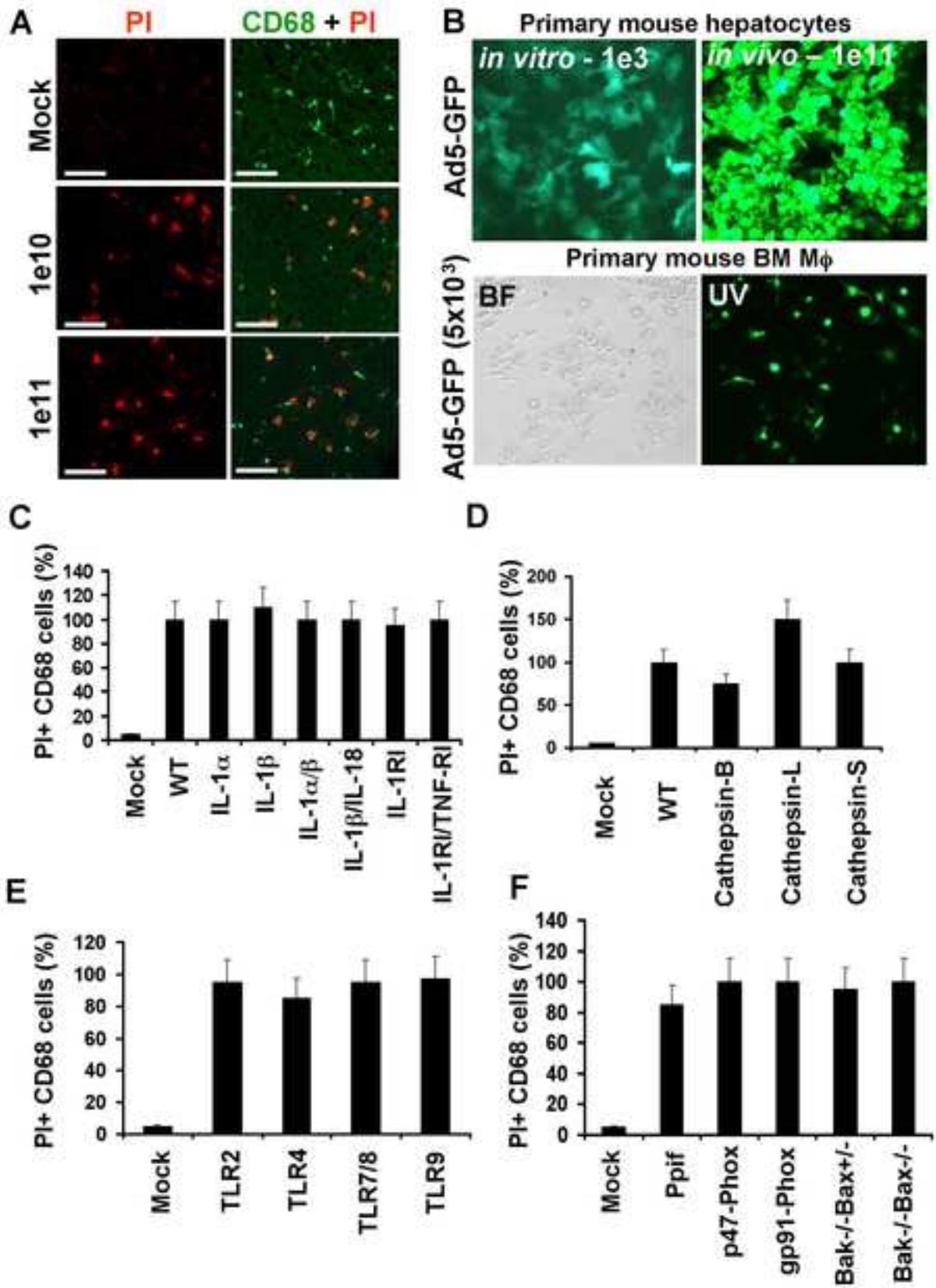

Supplemental figure 1.

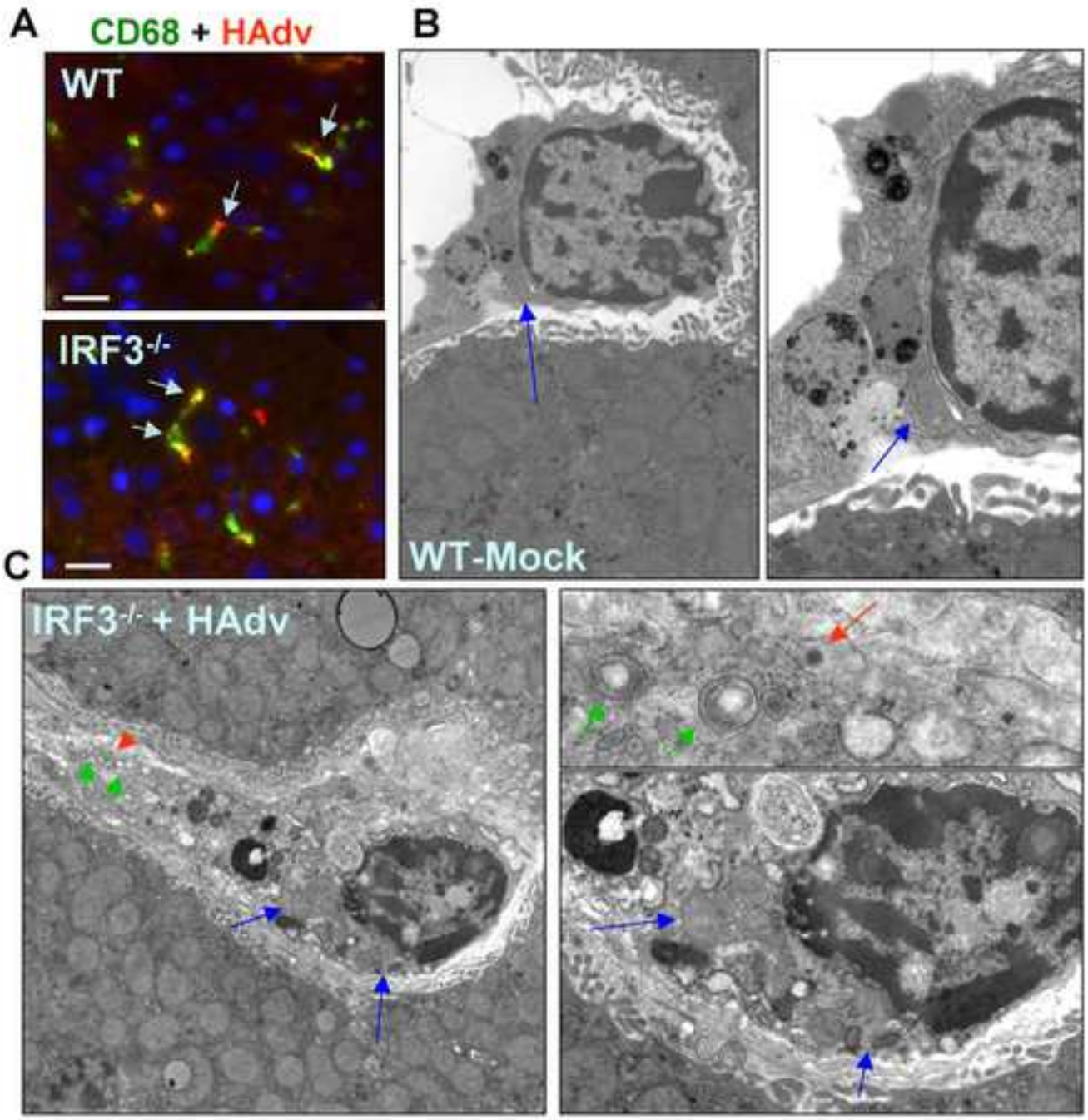

Supplemental figure 2.

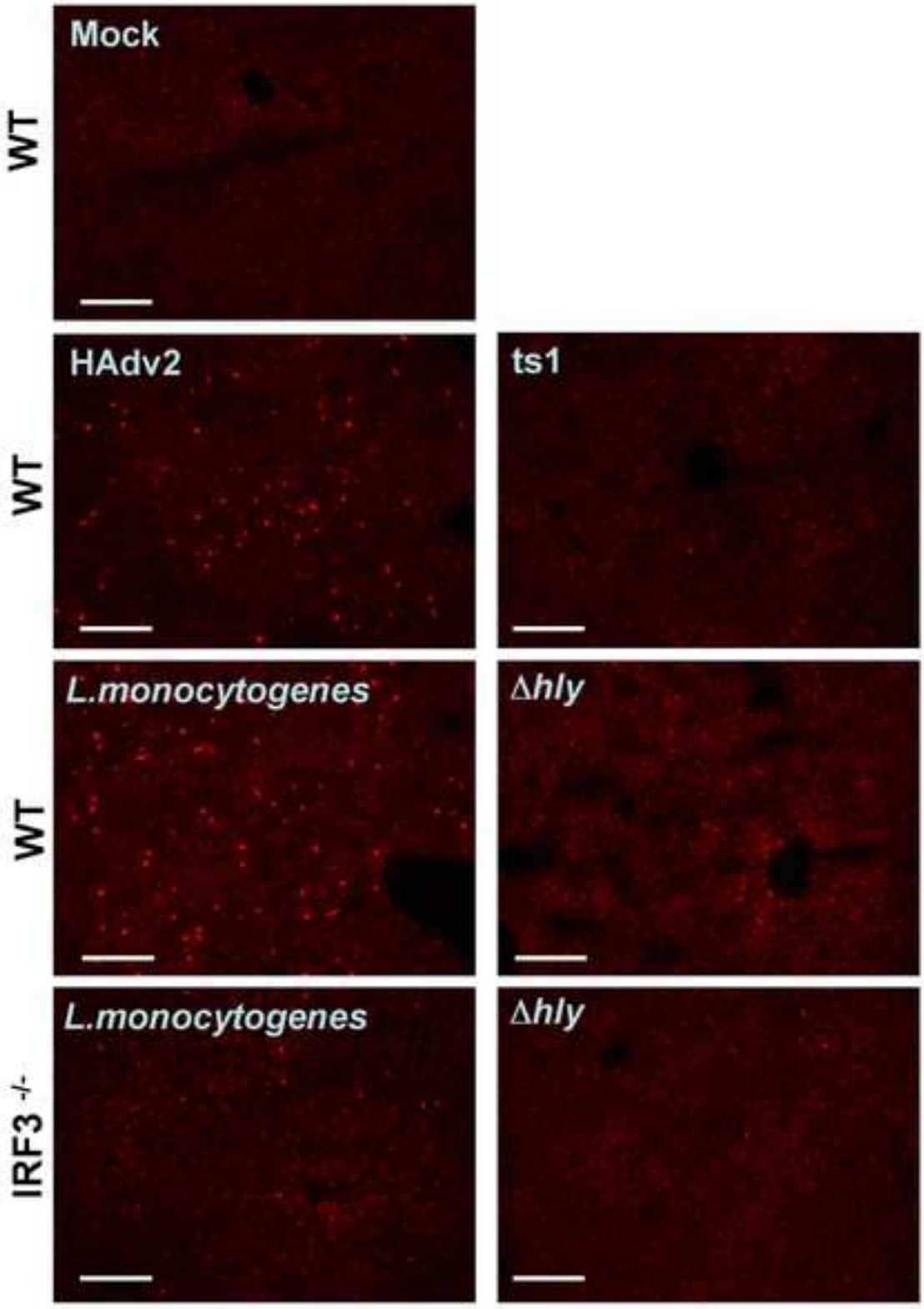

Supplemental figure 3.

Mouse Strain	Mutated Gene	Reference
Caspase-1/11-KO	*Caspase-1* and *Caspase -11*	(Kuida et al., 1995)
Caspase-2-KO	*Caspase-2*	Stock #7899, Jackson Laboratories
Caspase-3-KO	*Caspase-3*	Stock #6233, Jackson Laboratories
Caspase-6-KO	*Caspase-6*	Stock #6236, Jackson Laboratories
Caspase-7-KO	*Caspase-7*	Stock #6237, Jackson Laboratories
Caspase-8-flox/flox	*Caspase-8*	(Salmena et al., 2003)
Caspase-8-flox/flox	Caspase-8	(Ch'en et al., 2008)
ASC-KO	*Pycard*	(Mariathasan et al., 2004)
RAIDD-KO	*Cradd*	(Berube et al., 2005)
RIP3-KO	*Ripk3*	(Newton et al., 2004)
RIP3/Caspase-8	*Ripk3 and Casp8*	(Oberst et al., 2011)
MyD88-KO	*Myd88*	(Kawai et al., 1999)
TRIF-KO	*Ticam1*	Stock #5037, Jackson Laboratories
Cathepsin-B-KO	*Ctsb*	(Vasiljeva et al., 2008)
Cathepsin-L-KO	*Ctsl*	(Roth et al., 2000)
Cathepsin-S-KO	*Ctss*	(Shi et al., 1999)
IRF3-KO	*Irf3*	(Sato et al., 2000)
IPS1/MAVS/VISA-KO	*Mavs*	005, Seth et al, 2005, Xu et al, 2005, Meyl
DAI	*Zbp1*	(Ishii et al., 2006)
STING-KO (Gt/Gt)	*Tmem173*	(Sauer et al, 2011)
IL-1α-KO	*Il1a*	(Horai et al., 1998)
IL-1β-KO	*Il1b*	(Shornick et al., 1996)
IL-1α/β-KO	*Il1a* and *Il1b*	(Horai et al., 1998)
IL-1β/IL-18-KO	*Il1b* and *Il18*	(Sarkar et al., 2006)
IL-1RI-KO	*Il1r1*	Stock #3245, Jackson Laboratories
IL-1RI/TNF-RI-KO	*Il1r1* and *Tnfrsf1a*	Stock #3244, Jackson Laboratories
LyzM-CRE	-	Stock # 4781, Jackson Laboratories
TLR2	*Tlr2*	Stock #4650, Jackson Laboratories
TLR4	*Tlr4*	(Hoshino et al., 1999)
TLR7/8	*Tlr7* and *Tlr8*	(Hemmi et al., 2002)
TLR9	*Tlr9*	(Hemmi et al., 2000)
PPIF	*Ppif*	Stock #9071, Jackson Laboratories
gp91phox/NOX2	*Cybb*	Stock #2365, Jackson Laboratories
p47phox/NOXO2	*Ncf1*	Stock #4742, Jackson Laboratories
Bak-/-Bax*fl/fl*	*Bak and Bax*	Stock #6329, Jackson Laboratories

an et al, 2005)